Covalent Organic Frameworks

DOI: 10.1002/anie.201108462

Internal Functionalization of Three-Dimensional Covalent Organic Frameworks**

*David N. Bunck and William R. Dichtel**

Covalent organic frameworks (COFs) represent an emerging class of porous crystalline materials composed of light elements,[1] typically C, N, O, and/or B, that crystallize into two-dimensional (2D) layered structures or three-dimensional (3D) networks.[2,3] The nearly eclipsed structures[4,5] of most 2D COFs give rise to high intrinsic charge mobilities[6] and their recent synthesis as oriented thin films[7] portends their use in optoelectronic and energy-storage devices. In contrast, few 3D COFs have been crystallized, and despite exhibiting exceptionally high surface areas ($>4000\ m^2\,g^{-1}$) and record low densities ($0.17\ g\,cm^{-3}$), these networks have no well-developed applications.[8] Functionalizing the interior of 3D COFs might harness these desirable properties to provide structurally precise platforms for catalysis,[9] separations,[10] and the storage and release of molecular payloads.[11] However, no functionalized 3D COFs have been reported, while the functionalization of 2D COFs has been limited to alkyl chains.[12] Postsynthetic functionalization of related metal–organic frameworks (MOFs) relies on incorporating reactive groups,[13] such as alkynes[14] or amines,[15] on the organic linkers, but these moieties are not readily incorporated onto symmetric, polyvalent 3D COF building blocks.

Herein we report a general approach to functionalize 3D COFs using a new monomer-truncation strategy. A tetrahedral building block, which self-condenses to form the 3D network known as COF-102[2] (Scheme 1a), was modified such that one of its four arylboronic acid moieties is replaced with an arbitrary functional group. The resulting trigonal tris(boronic acid) is co-condensed with the parent tetrahedral monomer to provide functionalized COF-102 (Scheme 1b). The degree of functionalization is determined by the feed ratio of the two monomers and tolerates relatively high loadings of the truncated monomer (>30%), while the crystallinity, permanent porosity, and high surface area of the unfunctionalized material are maintained. This method also requires no modification of the solvothermal growth conditions used to crystallize COF-102. The truncated monomer is incorporated throughout the lattice, rather than on the crystallite surface, which might be unexpected given the reversible bond-forming conditions employed in COF synthesis.[16] However, growth conditions that produce crystalline materials are optimized empirically, and COF nucleation and growth processes are poorly understood. Our results indicate that boroxine hydrolysis is too slow to liberate truncated monomers from the COF-102 interior, thus their pendant functionality is distributed throughout the material.[17]

Dodecyl-functionalized COF-102 (COF-102-C_{12}) was obtained by condensing mixtures of **1** and **2** under solvothermal conditions (mesitylene/1,4-dioxane 1:1 v/v, 90 °C, 24 h). Samples of COF-102-C_{12} were isolated as microcrystalline powders by filtration and were activated under vacuum at 90 °C for 13 h. Fourier transform infrared (FTIR) spectra of activated COF-102 and COF-102-C_{12} were indicative of boroxine-linked materials, as judged by the intense B–O stretch at $1343\ cm^{-1}$ and attenuated O–H stretch relative to the analogous bands of their boronic acid precursors (Figure 1a). These spectra are consistent with those previously reported. The spectrum of a COF-102-C_{12} sample containing a 27% loading of the dodecyl-functionalized monomer **2** showed stretches for $C(sp^3)$–H bonds at $2900\ cm^{-1}$ not observed in the unfunctionalized COF-102 samples. COF-102-C_{12} samples also typically showed more intense residual O–H stretches, which we attribute to dangling boronic acid moieties opposite the dodecyl chains in the lattice. Overall, these spectra indicate that the co-condensation strategy produces a dodecyl-functionalized, boroxine-linked material similar to COF-102.

The percent incorporation of **2** into the COF-102-C_{12} lattice (T_{C12}) was evaluated by ^{1}H NMR spectroscopy after the material was digested in CD_3CN/D_2O (3:1 v/v). The ratio of **1**:**2** was determined by comparing the integration of the resonance at 0.84 ppm, corresponding to the -CH_3 protons of the dodecyl chain, to that at 7.25 ppm, corresponding to an aromatic proton found in both monomers (Figure 1b). The T_{C12} values calculated using this approach were very close to the feed ratios of the monomers used in the COF-102-C_{12} synthesis, up to feed ratios of 33%. Higher feed ratios (50%) still produced crystalline COF-102-C_{12}, albeit with T_{C12} levels that did not exceed 37%. This loading level might represent an upper limit for incorporating truncated monomers into the COF-102 lattice, in which the truncated building block comprises more than one-third of the network. In preliminary experiments, we isolated **2** as an amorphous boroxine-linked network instead of as a monomeric tris(boronic acid). When co-condensed with **1**, the boroxine form of **2** provided low T_{C12} values, further suggesting that boroxine hydrolysis is slow

[*] D. N. Bunck, Prof. Dr. W. R. Dichtel
Department of Chemistry and Chemical Biology, Cornell University
Baker Laboratory, Ithaca, NY 14853 (USA)
E-mail: wdichtel@cornell.edu

[**] This research was supported by startup funds provided by Cornell University, the NSF CAREER award (CHE-1056657), and a 3M Nontenured Faculty Award. We also made use of the Cornell Center for Materials Research (CCMR) facilities which are supported by the NSF Materials Research Science and Engineering Centers (MRSEC) program (DMR-1120296). D.N.B. acknowledges the award of a Graduate Research Fellowship from the NSF.

Supporting information for this article is available on the WWW under http://dx.doi.org/10.1002/anie.201108462.

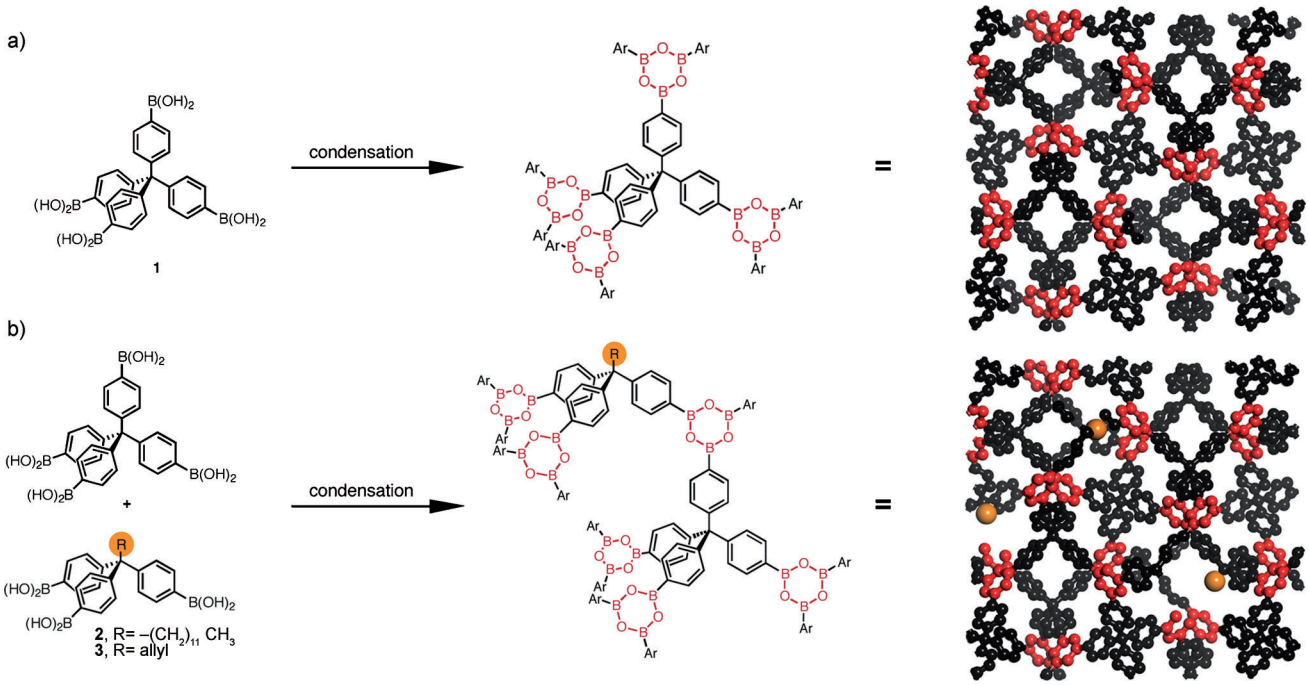

Scheme 1. a) The self-condensation of tetra(boronic acid) **1** yields the boroxine-linked network known as COF-102. b) Co-crystallization of **1** with truncated monomer **2** or **3** produces internally functionalized 3D COFs.

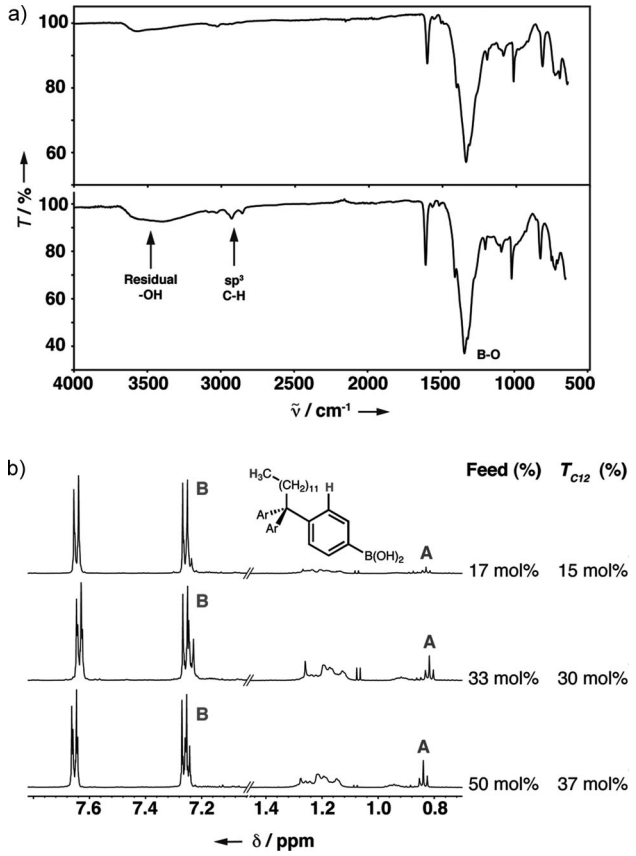

Figure 1. a) FTIR spectra of unfunctionalized COF-102 (top) and COF-102-C_{12} (T_{C12} = 27%, bottom). b) Quantitative partial ^{1}H NMR spectra (CD_3CN/D_2O, 500 MHz, 293 K) of digested COF-102-C_{12} samples used to determine the percent loading of **2** (T_{C12}).

relative to the rate of COF-102 growth. Monomer **2** was obtained as a tris(boronic acid) following lyophilization from wet 1,4-dioxane, and these samples consistently gave T_{C12} values similar to the monomer feed ratio.

COF-102-C_{12} is formed as a microcrystalline powder with an powder X-ray diffraction (PXRD) pattern identical to that of unfunctionalized COF-102, indicating that the functionalized material adopts the same network structure (Figure 2). For example, the PXRD pattern of a COF-102-C_{12} sample with a relatively high loading of **2** (T_{C12} = 24%) exhibits peaks ($Cu_{K\alpha}$) at 2θ = 7.9, 9.2, 12.1, 13.0, 14.5, 15.2, and 16.0° corresponding to the (211), (220), (321), (400), (420), (332), and (422) reflections. This powder diffraction pattern is nearly identical to that obtained for activated, unfunctionalized COF-102 and matches that previously reported. PXRD

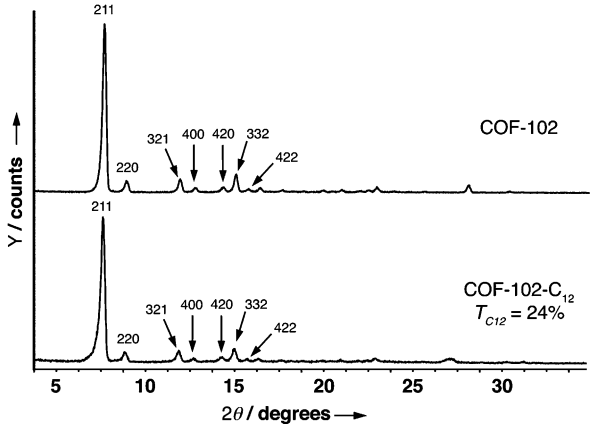

Figure 2. PXRD patterns of activated a) COF-102 and b) COF-102-C_{12} (T_{C12} = 24%).

patterns of COF-102 and COF-102-C_{12} obtained prior to activation show consistent differences in the intensities of their Bragg peaks relative to the patterns shown in Figure 2 (see the Supporting Information). COF-102-C_{12} samples with $T_{C12} \leq 24\,\%$ displayed similar PXRD patterns after activation. Materials with T_{C12} above this value (34 % and 37 %) showed similar diffraction patterns prior to activation, indicating formation of the crystalline network. However, activating these samples gave rise to amorphous materials, suggesting the decreased stability of these networks at the highest loading levels.[5] Scanning electron micrographs of unfunctionalized COF-102 and COF-102-C_{12} ($T_{C12} = 37\,\%$, Figure 3) show indistinguishable spherulites. These micrographs suggest that the truncated monomer **2** is distributed throughout the COF-102-C_{12} lattice, because differences in spherulite size would be expected if **2** was confined exclusively to the exterior surface at this loading level.

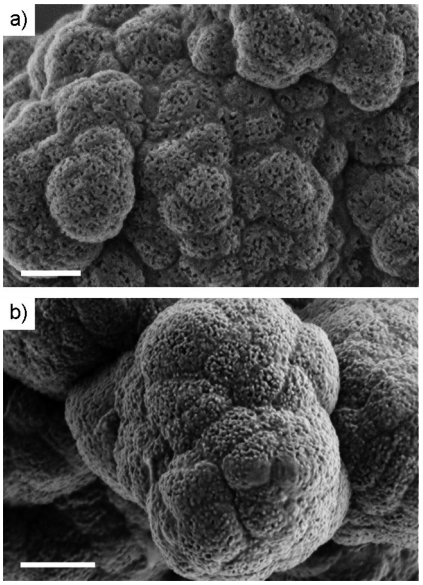

Figure 3. Scanning electron micrographs of a) unfunctionalized COF-102 and b) COF-102-C_{12} ($T_{C12} = 37\,\%$). Scale bars are 300 nm.

Gas-adsorption isotherms (N_2 and Ar) indicate that COF-102-C_{12} samples exhibit permanent porosity and high surface area that approach those of COF-102. Activated samples of COF-102-C_{12} with $5\,\% \leq T_{C12} \leq 24\,\%$ show Type I N_2-adsorption isotherms with a single adsorption into the pores at low relative pressure ($P/P_o < 0.10$, see the Supporting Information). Desorption is fully reversible with no observed hysteresis. The Brunauer–Emmett–Teller (BET) surface area model was applied to the $0.01 < P/P_o < 0.27$ region to provide the surface areas (S_{BET}) plotted in Figure 4a as a function of T_{C12}. These data indicate that COF-102-C_{12} samples retain high surface areas ($> 2000\ m^2\,g^{-1}$) that are inversely proportional to T_{C12}. By expressing this decrease as a percentage, the reduction in S_{BET} (S_{red}) scales linearly with T_{C12} with a slope of 1.01. Nonlocal density functional theory (NLDFT) analysis of the Ar-adsorption isotherms provided identical pore size distributions for unfunctionalized COF-102 and all COF-102-C_{12} samples and indicated a pore width

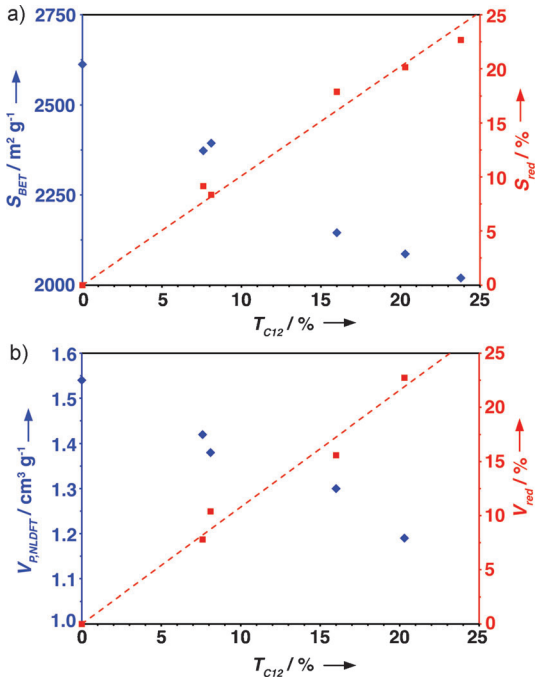

Figure 4. a) BET surface area (S_{BET}, N_2 adsorption, 77 K, blue points) and its percent reduction (S_{red}, red points) plotted as a function of the loading of **2** (T_{C12}). b) Cumulative pore volume ($V_{p,NLDFT}$, Ar adsorption, 87 K, blue points) and percent reduction in pore volume (V_{red}, red points) plotted as a function of T_{C12}. For the gas-adsorption isotherms corresponding to these data, see the Supporting Information.

of 12 Å (see the Supporting Information). The total pore volume ($V_{P,NLDFT}$) also decreases (Figure 4b) as a function of loading level. The percent volume reduction (V_{red}) scales linearly with T_{C12} with a slope of 1.08. The trends of reduced S_{BET} and $V_{P,NLDFT}$ with increased T_{C12} suggest that the dodecyl chains occupy the interior pore volume of the COF.

By employing the allyl-functionalized monomer **3**, COF-102-allyl was synthesized with a loading level (T_{allyl}) of 23 %. FTIR and PXRD indicated that COF-102-allyl is a boroxine-linked network similar to COF-102-C_{12}. Its pendant olefin is amenable to staining using OsO_4, which provides increased contrast in transmission electron micrographs. Samples of COF-102 and COF-102-allyl were exposed to OsO_4 vapor for 15 min. During this time both frameworks darkened in color, suggesting uptake into both materials. The samples were next placed under high vacuum to remove adsorbed OsO_4. While under vacuum, the unfunctionalized COF-102 lightened in color, while the COF-102-allyl sample remained dark, suggesting selective functionalization of its alkene moieties. Each COF was suspended in an epoxy resin, which was cured and microtomed to 60 nm thickness. The crystallites of Os-stained COF-102-allyl and COF-102 are similar in size and shape, but the allyl-functionalized crystallites are uniformly darker (Figure 5). The presence of Os was confirmed by energy dispersive X-ray microanalysis (EDX), and the COF-102-allyl samples consistently showed more intense Os signals than COF-102 samples. These observations suggest that the allyl moieties are distributed throughout the crystallite and are accessible to OsO_4 vapor.

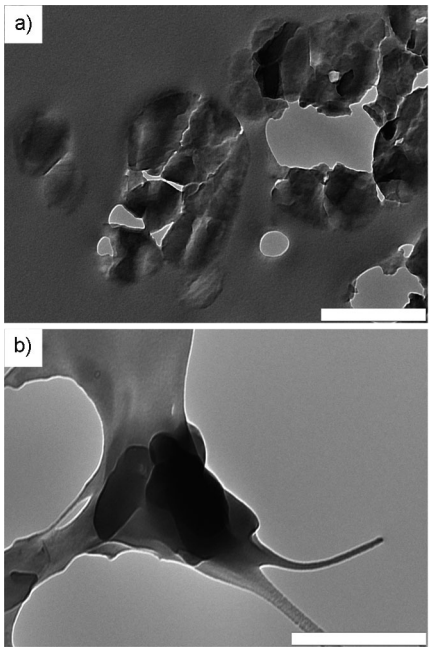

Figure 5. Transmission electron micrographs of microtomed samples (60 nm thickness) of a) unfunctionalized COF-102 and b) COF-102-allyl (T_{allyl} = 22%) suspended in epoxy after the OsO_4 staining procedure. Scale bars are 500 nm.

Finally, we evaluated the accessibility of the pores of COF-102 and COF-102-C_{12} to dissolved organic guests using pyridinium iodide **10** as a probe (Figure 6). Compound **10** exhibits a solvatochromic charge-transfer (CT) absorbance whose λ_{max} in various solvents forms the basis of the solvent polarity index known as the Z-scale.[18] Equal masses of COF-102 and COF-102-C_{12} (T_{C12} = 20%) were suspended in solutions of **10** dissolved in anhydrous CH_3CN (6.5 mL, 0.035 M). After 26 h, excess solution was removed and the COF samples were dried under high vacuum. Diffuse-reflectance UV/vis spectra of the two samples show the CT band of **10** as a broad shoulder of the COF aromatic absorbances (Figure 6). These absorbance bands are distinct from those of a sample of COF-102 physically mixed with **10**. These data indicate that **10** is loaded into the pores of both COF-102 and COF-102-C_{12} from solution and that both

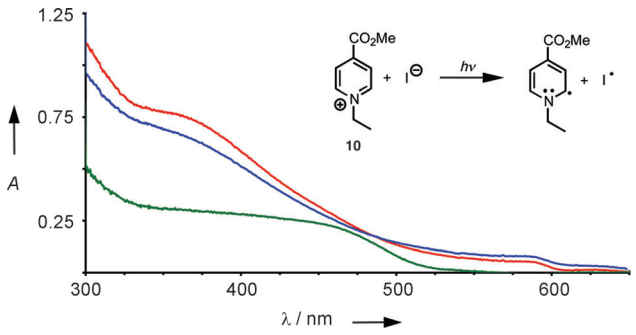

Figure 6. Diffuse reflectance UV/vis spectra of equal masses of unfunctionalized COF-102 (red trace) and COF-102-C_{12} (T_{C12} = 20%, blue trace) loaded with solvatochromic dye **10**, and of a physical mixture of unfunctionalized COF-102 and **10** (green trace).

materials feature distinct interior microenvironments. The COF-102 and COF-102-C_{12} samples take up comparable amounts of **10**, with slightly lower loading observed for the functionalized material. This difference is consistent with their gas-adsorption data, which also showed lower specific surface area as a function of T_{C12}. Finally, the similar appearance of the CT band of **10** in the functionalized and unfunctionalized COFs suggests that their interiors are similar, perhaps because the probe molecules preferentially reside in the unfunctionalized pore volume of COF-102-C_{12} rather than in pores already containing the dodecyl chains.

Here we have demonstrated a modular and versatile strategy to functionalize the interior of 3D COFs by co-condensing tetrahedral and truncated, trigonal monomers. The functionalized materials tolerate high loading levels of the truncated building blocks while retaining the crystallinity and high surface area of the parent 3D COFs. We are currently expanding the generality of this approach to other COF linking chemistries and developing these materials for applications in catalysis and payload release. It should also be noted that many of the tools commonly used to characterize COFs are surprisingly insensitive to the presence of high loadings of the functionalized monomers (which can be considered as defects). While the crystallinity of COFs derives from reversible bond formation, our results show that these exchange processes are not rapid enough to preclude incorporation of a truncated monomer into the lattice interior. Although the relative rates of bond formation and exchange processes during COF synthesis are not generally understood, control of these parameters, in concert with our truncated-monomer strategy, might furnish functionalized 3D COFs with designed crystallite morphology.

Received: December 1, 2011
Published online: January 16, 2012

Keywords: covalent organic frameworks · crystal engineering · microporous materials · polymers · self-assembly

[1] a) A. P. Côté, A. I. Benin, N. W. Ockwig, M. O'Keeffe, A. J. Matzger, O. M. Yaghi, *Science* **2005**, *310*, 1166; b) R. W. Tilford, W. R. Gemmill, H.-C. zur Loye, J. J. Lavigne, *Chem. Mater.* **2006**, *18*, 5296; c) S. Wan, J. Guo, J. Kim, H. Ihee, D. Jiang, *Angew. Chem.* **2008**, *120*, 8958; *Angew. Chem. Int. Ed.* **2008**, *47*, 8826; d) E. L. Spitler, W. R. Dichtel, *Nat. Chem.* **2010**, *2*, 672.
[2] H. M. El-Kaderi, J. R. Hunt, J. L. Mendoza-Cortés, A. P. Côté, R. E. Taylor, M. O'Keeffe, O. M. Yaghi, *Science* **2007**, *316*, 268.
[3] F. J. Uribe-Romo, J. R. Hunt, H. Furukawa, C. Klöck, M. O'Keeffe, O. M. Yaghi, *J. Am. Chem. Soc.* **2009**, *131*, 4570.
[4] a) E. L. Spitler, B. T. Koo, J. L. Novotney, J. W. Colson, F. J. Uribe-Romo, G. D. Gutierrez, P. Clancy, W. R. Dichtel, *J. Am. Chem. Soc.* **2011**, *133*, 19416; b) B. Lukose, A. Kuc, T. Heine, *Chem. Eur. J.* **2011**, *17*, 2388.
[5] W. Zhou, H. Wu, T. Yildirim, *Chem. Phys. Lett.* **2010**, *499*, 103.
[6] a) S. Wan, J. Guo, J. Kim, H. Ihee, D. Jiang, *Angew. Chem.* **2009**, *121*, 5547; *Angew. Chem. Int. Ed.* **2009**, *48*, 5439; b) X. Ding, L. Chen, Y. Honsho, X. Feng, O. Saengsawang, J. Guo, A. Saeki, S. Seki, S. Irle, S. Nagase, V. Parasuk, D. Jiang, *J. Am. Chem. Soc.* **2011**, *133*, 14510.
[7] a) E. L. Spitler, J. W. Colson, F. J. Uribe-Romo, A. R. Woll, M. R. Giovino, A. Saldivar, W. R. Dichtel, *Angew. Chem.* **2011**,

DOI: 10.1002/ange.201107070; *Angew. Chem. Int. Ed.* **2011**, DOI: 10.1002/anie.201107070; b) J. W. Colson, A. R. Woll, A. Mukherjee, M. P. Levendorf, E. L. Spitler, V. B. Shields, M. G. Spencer, J. Park, W. R. Dichtel, *Science* **2011**, *332*, 228.
[8] J. R. Holst, A. I. Cooper, *Adv. Mater.* **2010**, *22*, 5212.
[9] S.-Y. Ding, J. Gao, Q. Wang, Y. Zhang, W.-G. Song, C.-Y. Su, W. Wang, *J. Am. Chem. Soc.* **2011**, *133*, 19816.
[10] S. Han, Y. Wei, C. Valente, I. Lagzi, J. J. Gassensmith, A. Coskun, J. F. Stoddart, B. A. Grzybowski, *J. Am. Chem. Soc.* **2010**, *132*, 16358.
[11] P. Horcajada, T. Chalati, C. Serre, B. Gillet, C. Sebrie, T. Baati, J. F. Eubank, D. Heurtaux, P. Clayette, C. Kreuz, J.-S. Chang, Y. K. Hwang, V. Marsaud, P.-N. Bories, L. Cynober, S. Gil, G. Ferey, P. Couvreur, R. Gref, *Nat. Mater.* **2010**, *9*, 172.
[12] a) R. W. Tilford, S. J. Mugavero, P. J. Pellechia, J. J. Lavigne, *Adv. Mater.* **2008**, *20*, 2741; b) L. M. Lanni, R. W. Tilford, M. Bharathy, J. J. Lavigne, *J. Am. Chem. Soc.* **2011**, *133*, 13975.
[13] K. K. Tanabe, C. A. Allen, S. M. Cohen, *Angew. Chem.* **2010**, *122*, 9924; *Angew. Chem. Int. Ed.* **2010**, *49*, 9730.
[14] T. Gadzikwa, O. K. Farha, C. D. Malliakas, M. G. Kanatzidis, J. T. Hupp, S. T. Nguyen, *J. Am. Chem. Soc.* **2009**, *131*, 13613.
[15] a) K. K. Tanabe, S. M. Cohen, *Chem. Soc. Rev.* **2011**, *40*, 498; b) K. K. Tanabe, S. M. Cohen, *Angew. Chem.* **2009**, *121*, 7560; *Angew. Chem. Int. Ed.* **2009**, *48*, 7424.
[16] For a recent example of a defect-incorporation strategy used to functionalize metal–organic frameworks, see: T.-H. Park, A. J. Hickman, K. Koh, S. Martin, A. G. Wong-Foy, M. S. Sanford, A. J. Matzger, *J. Am. Chem. Soc.* **2011**, *133*, 20138.
[17] E. L. Spitler, M. R. Giovino, S. L. White, W. R. Dichtel, *Chem. Sci.* **2011**, *2*, 1588.
[18] E. M. Kosower, *J. Am. Chem. Soc.* **1958**, *80*, 3253.

